Nano Energy (2016) **19**, 511–521

Available online at www.sciencedirect.com

ScienceDirect

journal homepage: www.elsevier.com/locate/nanoenergy

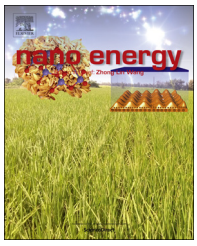

COMMUNICATION

Hierarchical nano-branched c-Si/SnO_2 nanowires for high areal capacity and stable lithium-ion battery

Hucheng Song, Hong Xiang Wang, Zixia Lin, Linwei YU*, Xiaofan Jiang, Zhongwei Yu, Jun XU*, Lijia Pan, Mingbo Zheng, Yi Shi, Kunji Chen

National Laboratory of Solid State Microstructures and School of Electronics Science and Engineering/ Collaborative Innovation Center of Advanced Microstructures, Nanjing University, Nanjing 210093, China

Received 8 May 2015; received in revised form 10 October 2015; accepted 28 October 2015
Available online 10 November 2015

KEYWORDS
Lithium ion battery;
Silicon NW;
SnO_2 NW;
Hierarchical structure

Abstract
Hierarchical structures, with a high mass-loading of nanostructured lithium (Li) storage medium grafted upon large *trunk* framework, represent a novel approach towards high capacity and stable Li-ion batteries. We here report a new hierarchical structure of crystalline Si nanowires (c-Si NWs) grafted upon ultra-long tin dioxide (SnO_2) NW trunks, where the latter frame up a large, conductive and stable architecture (i) to achieve a high mass-loading of c-Si NWs for Li-ion storage and (ii) to guarantee a good electric contact and fast charging process. The Si NWs branches are produced via a low-temperature vapor-liquid-solid (VLS) growth catalyzed by Sn droplets produced during a simple H_2 plasma treatment upon the SnO_2 trunks. Compared to other Si or SnO_2 NW-based anodes structures, the c-Si/SnO_2 NWs hierarchical structure demonstrates an outstanding performance with a high mass-load ($\sim$1.5 mg/cm^2) and a high areal capacity ($\sim$1.8 mAh/cm^2) after 100 cycles, without the use of any additional conductive polymer binder, highlighting the unique synergistic benefit of this hierarchical structure in boosting simultaneously the capacity and stability of Si-loaded Li-ion batteries.

Introduction

Seeking a high capacity and stable anode material has become one of the most challenging and demanding tasks in the develop of a new generation of high performance

*Corresponding authors.
E-mail addresses: yulinwei@nju.edu.cn (L. YU), junxu@nju.edu.cn (J. XU).

http://dx.doi.org/10.1016/j.nanoen.2015.10.031
2211-2855/

lithium ion batteries (LIBs) [1,2]. Among a wide variety of material choices, silicon (Si) and tin (Sn) are outstanding candidates thanks to their high theoretical charge capacities (Si, 4200 mAh/g and Sn, 994 mAh/g). However, lithium insertion and extraction in bulk Si anodes are always accompanied with a large volume change that thus causes a huge internal stress and quickly pulverization [3]. Various nanostructured Si or Sn-based anode frameworks, including nanoparticles (NPs) [4-6], nanowires (NWs) [7-10], nanotubes (NTs) [11,12], nanosheets [13,14], hollows/porous/hybrid nanostructures [15-18], have been explored to accommodate the huge volume change during cycling. For example, Yi Cui's group has demonstrated a high initial specific capacity (4200 mAh/g) based on short Si NWs anodes grown on stainless steels [9], with an improved stability compared to bulk c-Si thanks to a facile strain relaxation for tiny NWs. However, the capacity degrades quickly in the subsequent cycles due to irreversible crack formations within the Si NW cores [8]. Actually, taking Si NWs by themselves as both the storage medium and the conductive pathway could be somewhat contradictive, considering that the *radical* nature of lithium insertion into the c-Si, which poses a fundamental limit to Si NW-based Li-ion battery. This is particularly true for choosing ultra-long Si NWs (in order to have a high mass-load) as storage medium, because they have a higher likelihook of crack formation or breakage during initial cycles. To address this issue, a core-shell composite has been proposed with crystalline Si (c-Si) NWs [19] or carbon nanofibers [20] as the conductive cores, with an amorphous Si (a-Si) coating layer as the outer storage-medium shell. This is to assign different missions to the *core* and the *shell* materials. In doing so, a fast charging rate (6.8 A/g which is ~20 times of carbon) and a prolonged lifespan have been achieved, but at the expense of a largely decreased specific storage capacity (1000 mAh/g) compared to that of Si NWs anodes [9,19,20]. In parallel, SnO_2-based NWs are also investigated as a promising anode material, with a good electric conductivity and a high capacity compared to graphite [10,21,22]. For examples, P. S. Lee and co-workers reported a V_2O_5/SnO_2 core-shell nanostructure by coating V_2O_5 thin film over SnO_2 NWs, and demonstrated a high charging rate thanks to an efficient carrier transport in the SnO_2 cores; [23] W. Zhou and co-workers prepared nano-branched α-Fe_2O_3/SnO_2 hetero-structure by post-annealing hydrothermal growth of FeOOH precursor branches on SnO_2 NWs. Strikingly, these composite electrodes exhibit a higher specific capacity than that of any of the single component nanowires [24], emphasizing the unique benefits of such a branched hierarchical structure that requires still a better understanding.

In this work, we propose a new hierarchical Si NWs/SnO_2 NWs structures for lithium ion (Li-ion) battery, by grafting Si NW branches upon ultra-long conductive SnO_2 NWs trunks. The SnO_2 NWs help to (i) frame up a large 3D architecture to accommodate a high mass-loading of tiny Si NWs as the high capacity Li-ion storage medium, while (ii) serve as also efficient 1D electron transport channels to guarantee good electric contacts and fast charging/discharging. The Si NWs branches were grown in plasma enhanced chemical vapor deposition (PECVD) via a Sn-nanoparticle (NP) catalyzed vapor-liquid-solid (VLS) mechanism, where the Sn catalyst droplets can be produced conveniently by a simple H_2 plasma reduction of the SnO_2 NW sidewall. In comparison to other NW-based anode materials, including pure SnO_2 NWs, Sn-NP-decorated SnO_2 NWs and hydrogenated amorphous Si (a-Si:H) coated SnO_2 NWs core-shell structure, the Si/SnO_2 NWs hierarchical structure demonstrates a high initial specific capacity of ~3400 mAh/g with a greatly improved stability over 100 cyclings. We address also systematically the key controlling parameters for achieving an ideal Si NWs matrix upon conductive SnO_2 NWs and their underlying mechanisms.

Material and methods

Materials

Synthesis of SnO_2 NW: the SnO_2 NWs were directly grown upon the stainless steel substrates by a chemical vapor deposition (CVD) process, where a mixture of SnO_2 and carbon powder (molar ratio of 1.5:1) was placed at the center of a quartz tube as source materials, while the stainless steels substrates (pre-coated with a Au film of approximate 5–20 nm thick) were placed 3–10 cm away in the downstream of gas flow. The quartz tube was first pumped into a low vacuum of 1 KPa and kept in nitrogen gas flow for 10 minutes. Then, the source was heated to 940 °C at a ramping rate of 10 °C /min and then maintained for 2 h, while a carrier gas of 98% nitrogen and 2% oxygen was introduced at a flow rate of 30 sccm.

PECVD Growth of SiNWs upon SnO_2 NWs: the Si NWs were grown upon SnO_2 NWs by a Sn-catalyzed vapor-liquid-solid (VLS) process in a conventional plasma enhanced chemical vapor deposition (PECVD) system. First, a H_2 plasma treatment was carried out, with chamber pressure, gas flow rate and RF power density of 600 mTorr, 50 sccm and 76 mW/cm^2, respectively, for 6 min at 410 °C (nominal) to produce Sn droplets precipitation upon the SnO_2 NWs sidewall surface; Second, Si NW branches were grown mediated via a Sn-droplet-catalyzed VLS growth upon the SnO_2 NWs, when the substrate temperature was raised to 570 °C and a mixture gas of 5 sccm SiH_4 and 50 sccm H_2 was introduced, with chamber pressure of 600 mTorr and RF power of 76 mW/cm^2 for 60 min. For SnO_2/a-Si core-shell structure, amorphous silicon thin film was deposited with the same procedure except that there is no catalyst formation step, and thus no SiNW growth during the upon the SnO_2 NW.

Characterization methods

The morphology, structure and chemical composition of as-fabricated Si/SnO_2 nano-heterostructures were characterized by field emission scanning electron microscopy (FE-SEM, Sigma), Transmission electron microscopy (TEM, Tecnai G2 F20) and energy dispersive X-ray spectroscopy (EDX, Tecnai G2 F20).

Lithium ion battery assembly

The electrochemical properties of the samples were measured in CR2032 coin-type cells assembled in an argon-filled

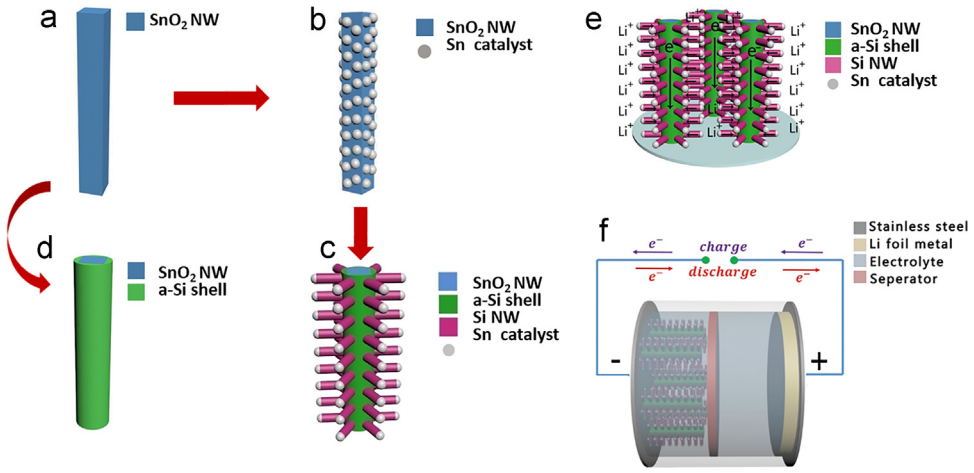

Figure. 1 Schematic diagrams showing the fabrication process of the Si/SnO_2 NW hierarchical structures, which include (a) SnO_2 NWs, (b) Sn-droplet-decorated SnO_2 NWs after hydrogen treatment, (c) Sn-catalyzed Si NWs growth on SnO_2 NW and (d) a-Si:H thin film coated SnO_2 NWs; (e) and (f) illustrate the final Si/SnO_2 NWs hierarchical structure grown on current collector (stainless steel substrate) and the lithium battery configuration, respectively.

glove box. The cells were formed using a Li metal negative electrode, with an electrolyte of 1 M $LiPF_6$ in a 1:1 ethylene carbonate anddiethyl carbonate mixture, a separator and a nanowire electrode, as schematically illustrated in Figure 1 (f). A galvanostatic cycling test of the assembled cells was carried out on a Land system (BT 2013A).

Results and discussion

Figure 1(a)-(d) illustrate briefly the synthesis procedure of the different hierarchical Si/SnO_2 NW structures investigated here: first, the SnO_2 NWs were produced by gold (Au)-catalyzed VLS growth in a thermal CVD tubular furnace upon stainless steel (SS) substrates (see Figure 1a); then, H_2 plasma treatment was applied to reduce superficially the SnO_2 NW sidewall to precipitate tiny Sn droplets upon the SnO_2 NW surface (see Figure 1b); In the next step, the SnO_2 NWs with Sn-droplet decoration were exposed to SiH_4 plasma for either coating an a-Si:H layer at a relatively lower temperature of 200 °C (see Figure 1c without Sn-NP), or growing Si NW branches upon the SnO_2 NW sidewall at a higher growth temperature of around 570 °C (see Figure 1d). The final hierarchical matrix and the lithium battery configuration realized upon the stainless steel substrate are schematically illustrated in Figure 1(e) and (f), respectively.

Figure 2(a) presents the scanning electron microscopy (SEM) image of the as-grown SnO_2 NWs, which have a diameter ranging from 40 nm to 100 nm and a length of more than several hundred microns. A low-magnification transmission electron microscopy (TEM) of a single SnO_2 NW is shown in Figure 2(b), with corresponding high-resolution TEM (HR-TEM) presented in Figure 2(c) showing clearly the lattice fringes of SnO_2 matrix (110) planes with a spacing of 0.33 nm [deduced from the diffraction spots in the selected area electron diffraction (SAED) analysis in the top-right inset of Figure 3(c)]. After H_2 plasma treatment at 5 W and 375 °C for 5 min, tiny Sn-NP droplets are formed on the SnO_2 NW sidewalls, as witnessed in the SEM image presented in Figure 2(d).

The Sn-NPs can serve as metal catalyst droplets in the next step to mediate the VLS growth of Si NW branches grafting upon the trunks of SnO_2 NWs, as illustrated in Figure 1(b) and (c) and shown in the SEM images in Figure 3. Close views of the fine Si NW branches are provided in Figure 3(b)-(d), where we found that the average diameter and the length of the Si NW branches vary as a function of the diameter of the SnO_2 NW backbones, as extracted and summarized in Figure 3(e). Specifically, when the SnO_2 trunk increases from ~250 nm to 750 nm in diameter, the Si NWs grown upon the NW sidewall shrink from d_{NW} ~108 nm to ~68 nm in diameter, while the length drops from L_{NW}~1000 nm to ~650 nm. This is accompanied by an increase of the surface density of the Si NWs branches grafted upon the SnO_2 trunks (for both the densities of unit length and unit sidewall surface area, as seen in Figure 3f). It seems that the diffusion and agglomeration kinetics upon the SnO_2 NW sidewall surface, which determines the density of the Sn catalyst droplet formation, is indeed sensitive to the local surface curvature (reciprocal of the trunk diameter). A probable explanation for that is the capillary surface tension of a curved SnO_2 NW sidewall could introduce an extra strain Gibbs energy *felt* by a sidewall-diffusing Sn atom, which can be written as

$$\delta G = \Omega_{Sn} \cdot P = \Omega_{Sn} \cdot \gamma / r_{NW}, \quad (1)$$

where γ and r_{NW} stand for the surface tension energy and radius of the SnO_2 NW, $P \equiv \gamma / r_{NW}$ the capillary pressure on a curved surface and Ω_{Sn} the atomic volume of Sn atoms, respectively. This in turns modifies the relative diffusion barrier height (E_b) and thus the diffusion coefficient of Sn atoms (D_{Sn}) on the NW sidewall by $D_{Sn} = D_0 e^{-\frac{E_b - \delta G}{kT}}$. As we know, the separation between self-agglomerated Sn-NPs (inverse of density) is proportional to the surface diffusion length of Sn atoms L_{Sn}, and the latter can be related to the diffusion coefficient by

$$L_{Sn} \sim \sqrt{D_{Sn}} = \sqrt{D_0}\, e^{-\frac{E_b - \Omega_{Sn} \cdot \gamma / r_{NW}}{2kT}} \sim 1/density \quad (2)$$

So, it will be logic to expect that, a thinner SnO_2 NW with a higher local surface curvature could lead to a longer sidewall diffusion length, and thus lower surface density of

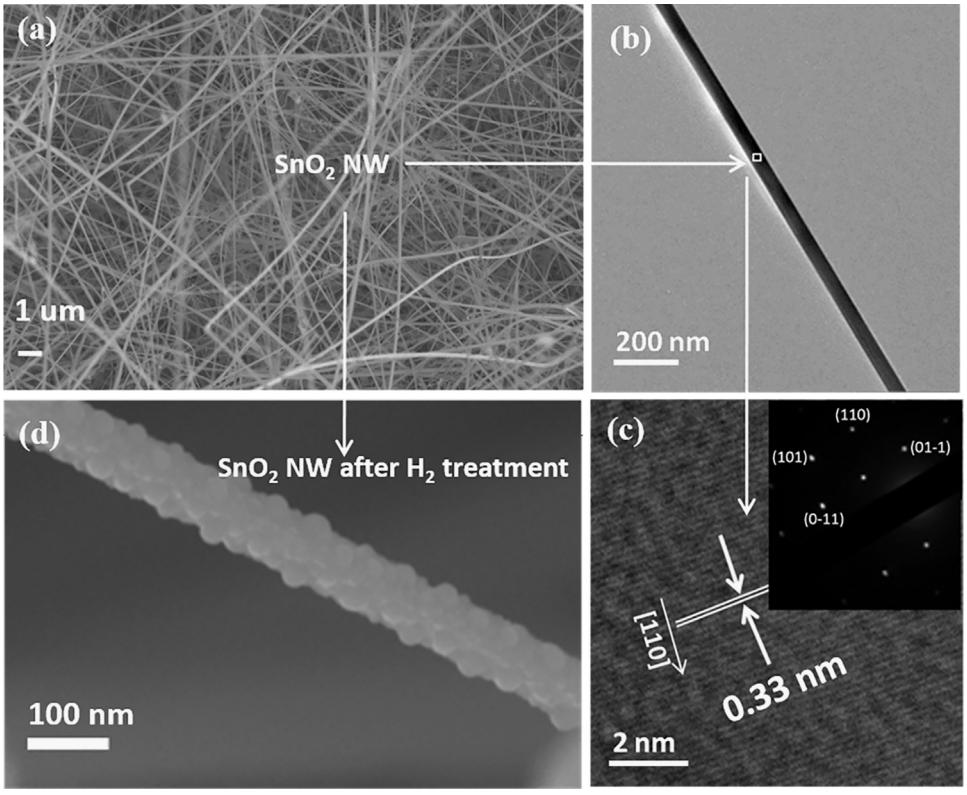

Figure. 2 (a) SEM image of SnO_2 NWs directly grown on stainless steel substrate; (b) Low-magnification TEM image of a single SnO_2 NW, and its corresponding high-resolution TEM analysis and selected area electron diffraction (SAED) patterns shown in (c) and the top-right inset; (d) the SEM image of a single SnO_2 NW after H_2 plasma treatment, with clear Sn droplet formation upon the SnO_2 NW's sidewall.

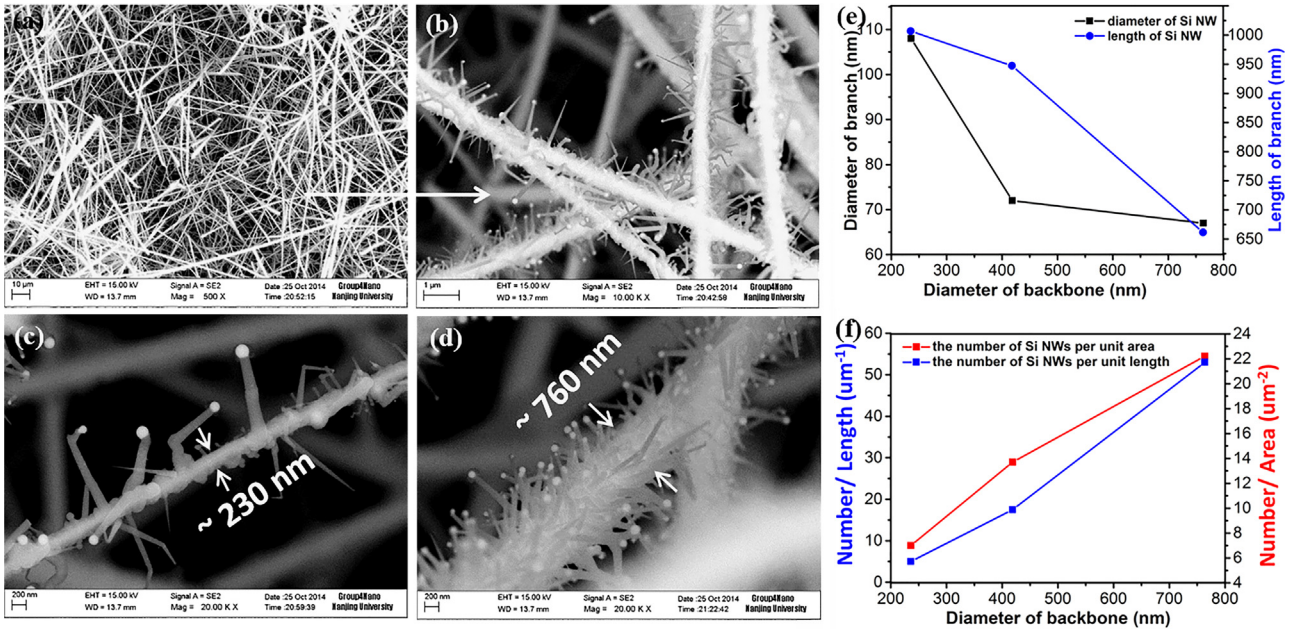

Figure. 3 (a) shows the SEM image of the Si/SnO_2 nanowires (NWs) hierarchical structures, with Si NWs grafting upon the SnO_2 NW trunks, with close views of the heterostructures complex provided in (b)–(d), revealing that the diameter, length, line density (Number/Line, in blue) and area density (Number/Area, in red) of the grafting Si NWs also vary as a function of the diameter of the SnO_2 NW-backbones, as summarized in the plots in (e) and (f).

Sn-NP (larger catalyst droplet, and thus thicker and longer Si NW branches on thinner SnO_2 NW trunk). Though the detail mechanism is still an open topic to investigate, we note that this unique aspect could imply an opportunity to tailor the density of Si NW branches catering for the need of optimal lithium battery design.

To assess the structural properties of the Si NWs branches grown upon the SnO_2 NW trunks, high-resolution TEM characterizations have been conducted to examine the crystallographic structure of NWs, as well as the hetero-interface between the SnO_2 NW backbone and the Si NW branches. As seen in Figure 4(a), on both sides of a SnO_2 NW, Si NW branches are grown with bright Sn droplets resting at the tips. High-resolution TEM characterization of the joint of the Si NW branch and the SnO_2 NW trunk, in Figure 4(b), shows that the crystalline matrices of the Si NW branch and the SnO_2 NW trunk meet abruptly at the root, and both of them are coated with a layer of a-Si: H (~8 nm on the Si NW and ~12 nm on the SnO_2 NW). Close examinations and analysis in Figure 4(b)-(d) help to confirm that the growth orientations of the SnO_2 NW trunk and the cubic Si NW branch are tetragonal SnO_2 [110] and cubic Si [311], respectively [25].

Figure 4(e) presents the Energy dispersive X-ray spectroscopy (EDS) elemental mapping analysis of the spatial distributions of Sn, Si and O elements among several Si NW branches on a SnO_2 NW backbone, with the extracted distribution profiles along two scan lines indicated in Figure 4(e) plotted Figure 4(f). As we can see, along the trace line marked by "1" on SnO_2 NW trunk, there is a high concentration of Sn precipitation over the main trunk of SnO_2 NW, accompanied with a surface-coating a-Si:H layer. Elemental profile analysis (line "2") along a grafted Si NW branch reveals a partially oxidized Sn droplet at the tip of Si NW, and on the surface of the Si NWs we observe a non-negligible Sn traces that could arise from the spreading of Sn catalyst liquid during the VLS growth [26].

The Si NW/SnO_2 NW hierarchical structure was then assembled into LIBs with a configuration illustrated in Figure 1(f). Figure 5(a) shows the initial discharging and charging curves, where a series of voltage plateau/or shoulder were identified at around 0.8–0.9 V in the first-

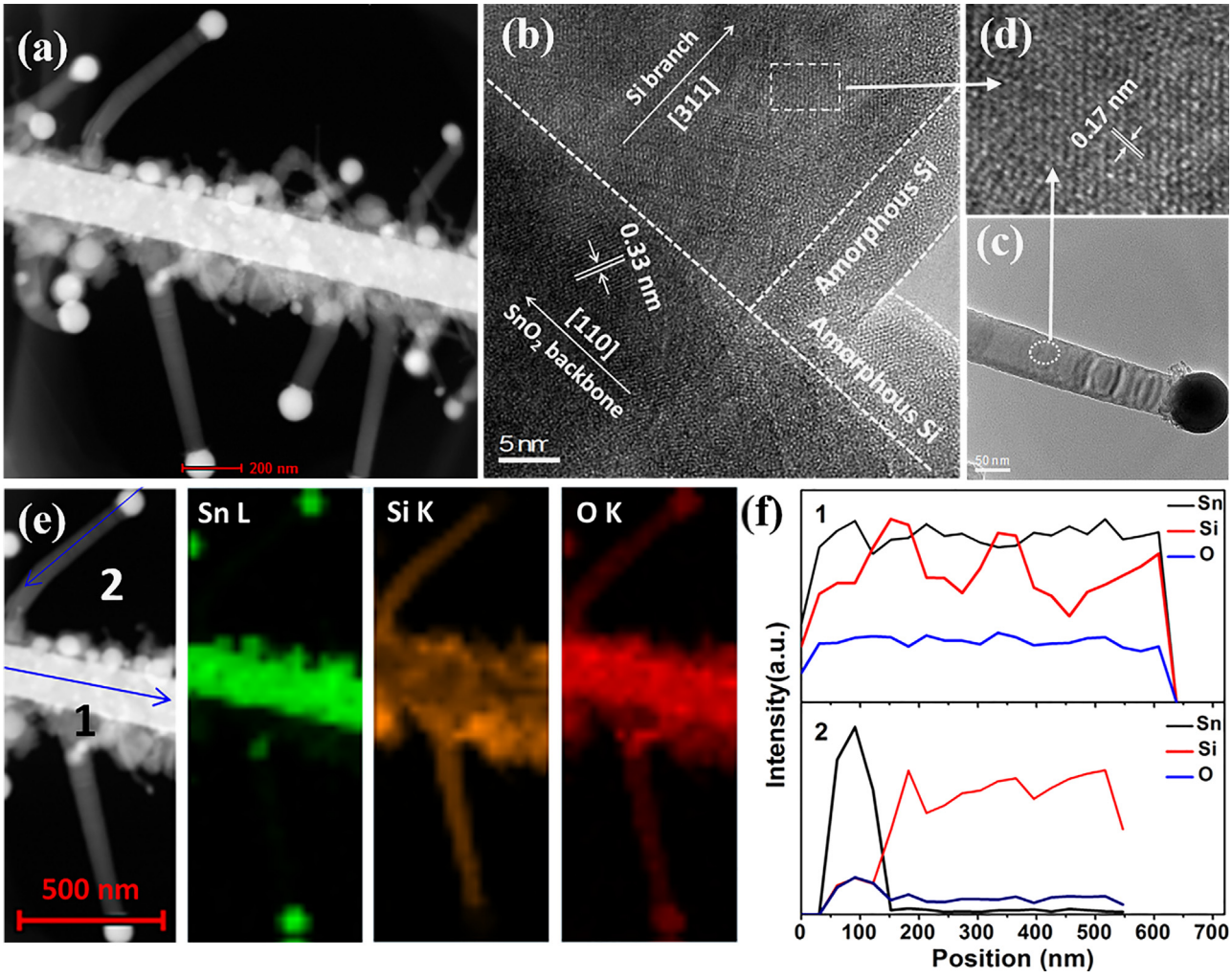

Figure. 4 (a) TEM images of the Si/SnO_2 hierarchical complex, and (b) High-resolution TEM characterizations of the Si NW/SnO_2 NW interface; (c) Bright-field TEM image of a single Sn-catalyzed Si NW branch with enlarged HR-TEM imaging in (d); (e) presents the elemental mapping images (of Si, Sn and O) over several Si NW branches on a SnO_2 NW, with corresponding line profiles, marked by "1" and "2", extracted and plotted in (f).

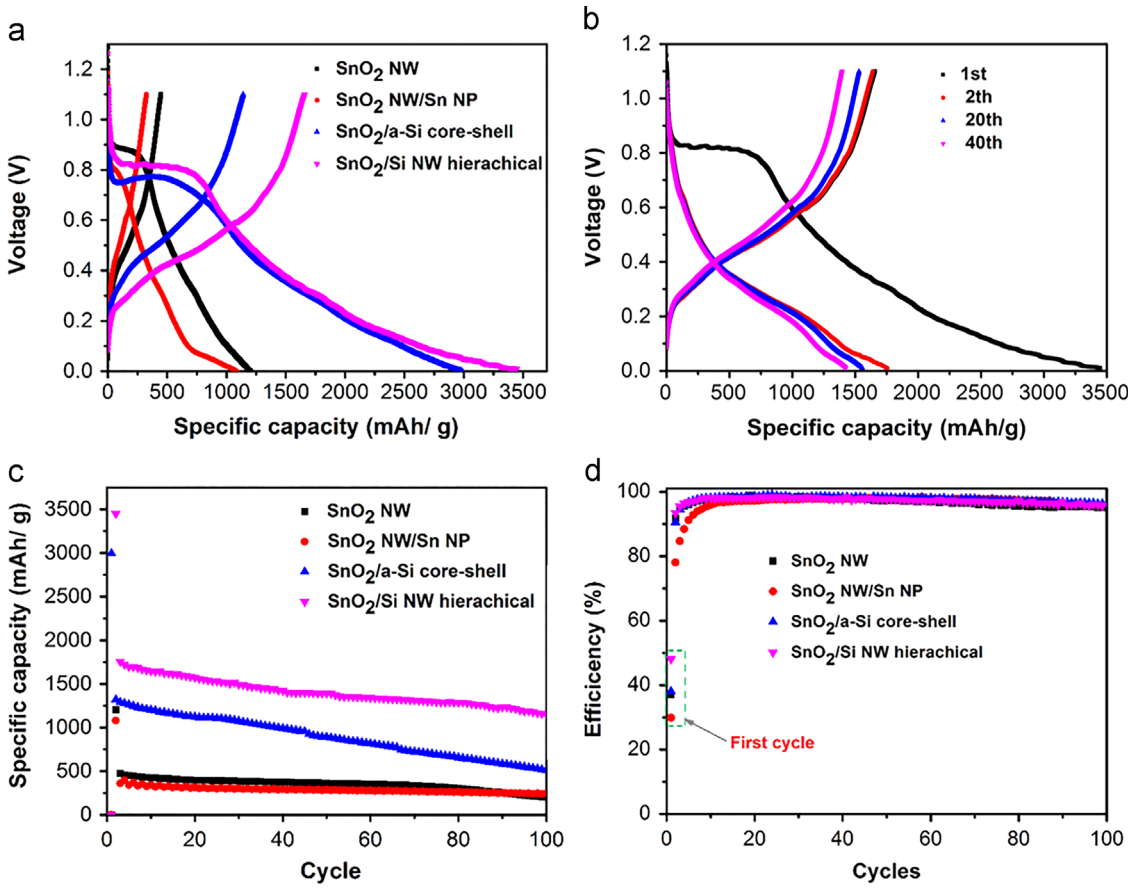

Figure. 5 Electrochemical cycling characterizations of the lithium ion batteries (LIB) with anode electrodes materials of bare SnO_2 NW, Sn NP-decorated SnO_2 NWs, a-Si-coated SnO_2 NWs, and Si NW-grafted SnO_2 NWs hierarchical structures: (a) Initial discharging/charging curves of the corresponding samples at a rate of C/10; (b) voltage profiles of the 1st, 2nd, 20th, 40th cycles of Si NW-grafted SnO_2 NWs hierarchical structures; (c) and (d) show the discharge capacities and columbic efficiencies (at C/10 rate) of four sample over 100 cycles, respectively.

cycle discharging curves among the four different anode samples, which can be assigned to the electrochemical reaction between Li-ions and the SnO_2 NWs and the oxidized Sn-NP at the tip of Si NWs [27,28], as described below,

$$SnO_2 + 2Li^+ + 2e^- \rightarrow SnO + Li_2O, \quad (3)$$

$$SnO + 2Li^+ + 2e^- \rightarrow Sn + Li_2O, \quad (4)$$

$$Sn + xLi^+ + xe^- \leftrightarrow Li_xSn (0 \le x \le 4.4), \quad (5)$$

Usually, the first two reactions are considered as irreversible and thus cause permanent decomposition of SnO_2 into Sn after the first discharge process, while the last one accounts for the reversible charging/discharging of the SnO_2 (or Sn)-based nanomaterial. We observe that the SnO_2 NWs sample after H_2 plasma treatment (to produce Sn-NPs decoration on sidewall) exhibits a lower first discharge specific capacity (to 1080 mAh/g) than that of pure SnO_2 NWs (1205 mAh/g). The reason for that could be twofold: first, during the H_2 plasma treatment, some tiny SnO_2 NWs with very thin diameter could be broken; second, the precipitated Sn could be lost via airborne pathway by forming volatile Stannane (SnH_4) and being pumped away. However, a slightly better cycling stability has been obtained for the Sn-NP decorated SnO_2 NW sample [see Figure 5(c) after 100 cycles], which could be attributed to an enhanced mechanical stability and larger expansion space enjoyed by the Sn-NPs as proposed by P. Madura's work [22].

When being coated with a thin layer of a-Si: H or grafted with VLS-grown Si NWs branches, a large incremental specific capacity can be achieved up to 3000 mAh/g or 3400 mAh/g, respectively. The voltage profiles of the Si/SnO_2 NW hierarchical structure at the 1st, 2nd, 20th and 40th cycle are showed in Figure 5(b), respectively. For the first discharge curve, the plateau around 0.83 V is observed, corresponding to the irreversible decomposition of SnO_2 However, in the next cycles, this discharge plateau around 0.8 V disappears and exhibits only little change from the 2nd to the 40th runs, indicating that the Si/SnO_2 NW hierarchical structure are quite stable during cycling. Compared to all the other NW structures, the Si/SnO_2 NWs hierarchical structure demonstrates largely improved cycle stability as witnessed in Figure 5(c).

Furthermore, this stability, by itself, does not degrade with the increase of charging/discharging rates from C/10 (~340 mAh/g), C/7 (~480 mAh/g) to C/5 (~780 mAh/g) during the initial 100 cycles, as shown in Supplementary Materials S1. This is indeed remarkable if we compare the

cycle stability of the a-Si:H coated SnO_2 NWs to that of the Si NWs-grafted SnO_2 NWs sample. Both of them have been loaded with more or less the same amount of Si contents, but loading the Si mass as superimposed NW branches has led to both a higher specific capacity and a better stability over its thin film-coated counterpart. Specifically, for the a-Si:H-coated SnO_2 NWs structure, the first discharge capacity can reach 3000 mAh/g, but suffers quickly a capacity drop to about 500 mAh/g after 100 cycles. This could be ascribed to the fracture of the outer a-Si:H coating shell caused by large volume expansion/contraction [19,20]. In contrast, *re-arranging* the Si mass-load into a high population of tiny Si NW branches connected to the SnO_2 NW trunks provides a roomy 3D architecture to accommodate the radical volume change. In addition, it is also noteworthy that the spare surface on SnO_2 NWs (between Si NW branches) are covered by a very thin a-Si:H layer [see Figure 4(b)], which is co-deposited during a plasma enhanced VLS-growth of Si NWs. This very thin a-Si:H layer could play a role, to some extent, in protection of the SnO_2 trunk for a better stability. As witnessed in Figure 5(b), after the first cycle, the capacity of the Si/SnO_2 NWs hierarchical structure was ~1770 mAh/g and maintained at ~1200 mAh/g after 100 cycles, corresponding to a retention rate of 67%. The rate performance of the Si NW-grafted hierarchical structure has also been tested at different charge/discharge current densities, ramping from 0.1 C (~420 mA/g) to 2.0 C (~8.4 A/g) and then back to 0.1 C (~420 mAh/g), with the capacity evolution curve displayed in Supplementary Materials S3. As we can see, the c-Si/SnO_2 hierarchical nanowire anode structure has been able to sustain high rate cycling (2.0 C) under high mass-loading (1.5 mg/cm^2) condition, with still a capacity recovery ratio of 80% after the high rate operations.

Furthermore, Figure 5(d) shows the Columbic efficiency (CE) of the LIBs with different NW anode materials. All these samples feature a low initial CE below <50%, caused by (i) the irreversible reaction of SnO_2 (on the exposed backbone or at the tip of Si NWs) with Li-ions in the first-cycle discharging; and ii) the formation of a SEI layer [29]. Among them, the Si/SnO_2 NWs hierarchical electrode exhibited the highest first CE close to 50%, compared to that of less than 40% for the other electrode materials. The reason behind could be: first, the a-Si:H layer coating could limit the direct lithiation of the SnO_2 NWs trunk; second, there has been reports that in the presence of Sn-NPs or Fe-NPs, Li_xO could be partially decomposed back into the Li-ions, making the Eq. (4) somewhat reversible [22,24]. To improve the first CE further, there has been report that a surface coating layer of ALD-deposited TiO_2 thin film [28] can help to promote the first CE of SnO_2 NWs LIBs from 45.2% to 57.9%.

The advantages of the Si/SnO_2 NW hierarchical anode structure could be summarized as, (i) first, a large and firmly attached mechanical support provided by the ultra-long SnO_2 NWs matrix, which are directly grown on current collector substrate serving as efficient electric pathways; (ii) second, during the growth of Sn-catalyzed Si NW in a PECVD system, there is also a plasma-enhanced co-deposited a-Si:H layer covering both the sidewall of SnO_2 NW trunk (even without Sn-NPs) and the root of the Si NWs, which could help to strengthen the adhesion between the Si NW-branches and the SnO_2 NW-backbones against large volume fluctuation during charging and discharging; (iii) third, plenty of free spaces among the high density but tiny Si NWs help to accommodate large volume expansion of Si and thus provide more active sites for lithium ions accesses; (iv) The SnO_2 NW cores are indeed more conductive than the grafted Si NWs, and thus provide an ideal and efficient conductive pathways to facilitate fast charge/discharge operation, without the need of conductive polymer binder. During lithiation process, when the inner SnO_2 cores could be reduced into far more conductive Sn, while being constraint by the outer Si-coating layer to keep the integrity and prevent breakage of the conductive pathway. This is indeed a unique synergistic effect of the c-Si NWs and SnO_2 nanowires, which can help to achieve simultaneously a higher rate performance and high mass-loading, in a 3D hierarchical NW framework with the aid of fine-tuned plasma coating/co-deposition technique.

Meanwhile, it is also important to emphasize that this hierarchical c-Si/SnO_2 NW structure provides a unique opportunity to combine the advantages of tiny c-Si NWs with a high specific capacity to a high mass-load framework of ultra-long SnO_2 NWs. In this way, we have achieved a high areal capacity of 1.8 mAh/cm^2 with a greatly improved stability, compared to those Si-based batteries as summarized in Table 1. To the best of our knowledge, this areal capacity demonstrated here is much higher than those based on Si or SnO_2 nanowire core-shell or nano-branch structures reported in the literature, as summarized in Table 1 [32-42]. In seeking even higher areal capacity density, we also tried to increase the overall mass-loading (while keeping more or less a constant Si or SnO_2 mass ratio), from 0.9 mg/cm^2 to 5.3 mg/cm^2, and present the cycling evolution of the areal capacity densities in Supplementary Materials S2. We found that, when a much higher initial areal capacity of 4.4 mAh/cm^2 is indeed achievable with a higher mass-loading of 5.3 mg/cm^2, the degradation becomes also faster that decreases to ~3.2 mAh/cm^2 after 30 runs of cycling. This could reflect a situation that a conformal coating or uniform Si NW grafting by PECVD deposition becomes difficult over a longer and more complex 3D SnO_2 framework, and thus the deep SnO_2 NW roots (unprotected by Si coating) are vulnerable to breakage during cycling. Of course, further investigation into this point is still needed to develop an optimal structural design or strategy.

In order to gain further insight of the improved cycling stability of the Si/SnO_2 NWs composited electrode, we continue to examine the microstructure and morphology of the hierarchical anodes after 160 cycles at 1.1 V by SEM and XRD. As seen in the SEM images in Figure 6(a)-(c), the Si NW branches become highly porous, as expected for high capacity Si matrix [30,31], but still remain attached to the SnO_2 NW backbones [see Figure 6(b)] after 160 cycles. In addition, the overall hierarchical structures are still well preserved, with clear and separated backbone framework and discernible Si NW branches and without significant aggregations. These observations provide straightforward and convincing evidences for the superiority of the c-Si/SnO_2 NW hierarchical structure to accommodate a large volume expansion/contraction during discharging/charging cycles. The microstructure after 160 cycles were also investigated by XRD characterizations before (black) and

Table 1 A summary and comparison of the mass-load, cycling stability and areal capacity performances of different one-dimensional SnO_2 and Si-based nanostructures reported in literature, in comparison to what achieved in this work:.

Materials	Structure	Mass load (mg cm^{-2})	Current Density	Cycles	Capacity after cycles (mAh g^{-1})	Areal capacity after cycles (mAh cm^{-2})	Reference
SnO_2 NR	1D nanorod array (D: 60 nm, L: 670 nm)	~0.88	~0.1 C	100	~580	0.51	[33]
SnO_2 NW	1D NW array (D:40-50 nm; L: 1 mm)	———	~0.78 Ag^{-1}	50	~510	———	[34]
SnO_2/Ni	Coating SnO_2 (~8 nm) on Ni nanofoam	~1.0	~0.5 Ag^{-1}	100	~500	0.5	[35]
V_2O_5/SnO_2	1D Core-Shell NW array	~1.1	~0.2 Ag^{-1} ~20 Ag^{-1}	100 100	~140 ~90	———	[23]
a- Fe_2O_3/SnO_2 NW	Hierarchical structure	————	~1.0 Ag^{-1}	30	~230	———	[24]
SnO_2/a-Fe_2O_3	1D Composite nanotube array	~0.75	~0.13 Ag^{-1}	50	~965	0.727	[32]
SnO_2 @Sn	1D SnO_2 NW covered with Sn nanoparticle	————	~0.1 Ag^{-1}	100	~814	————	[22]
SnO_2@Si/C	Core shell NW on Carbon	>0.5	~0.38 mA cm^{-2}	50	————	~1.39	[36]
Si NW	Directly grown on SS	~0.5	~C/20 Ag^{-1}	10	~3120	~1.5	[9]
c-Si NW/C	Core-shell NW net works	————	~0.4 Ag^{-1}	65	~600	————	[39]
c-Si @ a-Si	Core-shell NW array	————	~0.85 Ag^{-1}	100	~1060	————	[19]
a-Si @ CNF	1D core-shell NW array	~1.6	~0.5 Ag^{-1}	55	~1900	~3.0	[20]
MSC-Si/G	Nanohybrids on Cu foam	~1.0	~0.2 Ag^{-1}	100	~1500	~1.5	[37]
Si/CNT	Coaxial Nanofiber	~0.74	~0.2 C	100	~1700	~1.25 (22 um) ~0.26 (15 um)	[38]
a-Si/SnO_2 NW	Core-shell	~1.47	~0.3 Ag^{-1}	100	~500	~0.74	This work
c-Si /SnO_2 NW	Hierarchical structure	~1.5	~0.36 Ag^{-1}	100	~1200	~1.8	This work

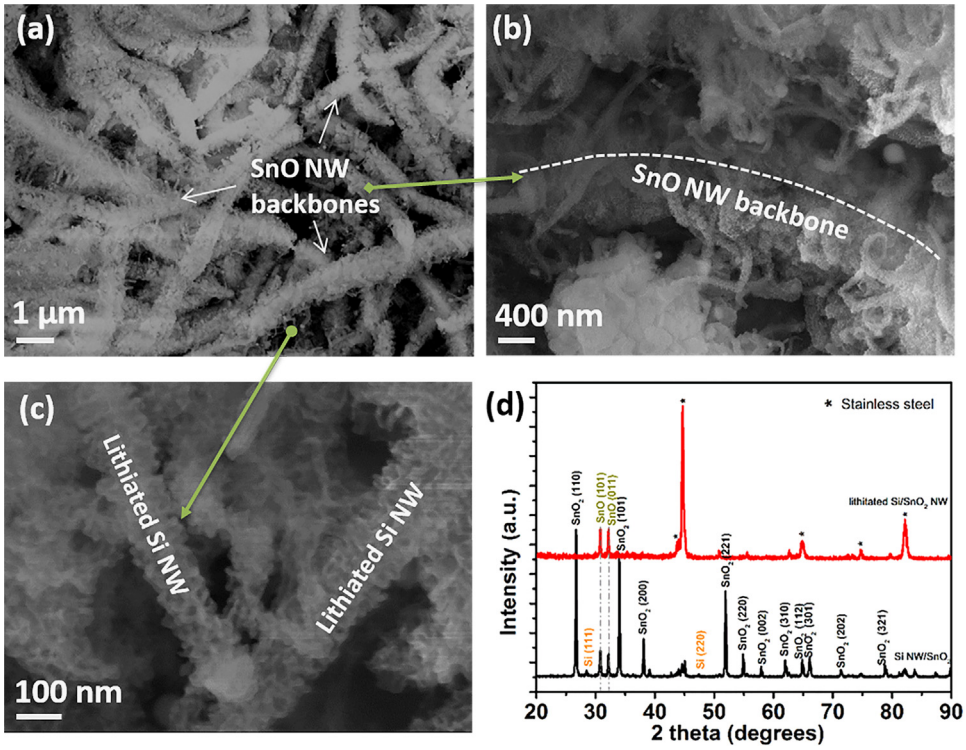

Figure. 6 Morphology and structural characterization of Si/SnO_2 NW composite electrode after 160 cycles: Low-magnification SEM of Si/SnO_2 NW (a); High-magnification SEM of lithiated SnO_2 backbone (b) and Si NW branch (c); (d) shows the XRD analysis of the Si/SnO_2 composite electrodes before (black) and after (red) 160 runs of lithiation.

after (red) lithiation in Figure 6(d). We observed that the initial SnO_2 (110) peaks located at diffraction angles of $2\theta = 26.71^\circ$ in SnO_2 NWs. After charging/discharging for 160 runs, two new peaks emerge at 30.27°, and 31.64° corresponding to the (101) and (011) orientations in crystalline SnO matrix. This indicates that the SnO_2 cores also participate in the lithiation process, while their geometry and framework can be well preserved, which is an important basis for achieving a better cycle stability for the hierarchical NW structure.

In summary, we have proposed a novel hierarchical Si/SnO_2 NW structures to achieve a high specific capacity and cycling stable (~3400 mAh/g at initial charging and ~1200 mAh/g after 100 cycling) Li-ion battery based on Si NWs branches grafted upon SnO_2 NWs backbone, fabricated in a conventional PECVD system without the use of additional polymer or carbon binders. Moreover, this hierarchical structure enables a high Si mass-loading (~1.5 mg/cm^2) and a high areal capacity (~1.8 mAh/cm^2), and exhibits excellent mechanical integrity after 100 cycling without any conductive agent and binder. We suggest that this hierarchical structure could also indicate a strategy applicable to other high capacity alloy-type anode material systems for developing a high performance next generation Li-ion battery.

Acknowledgments

This work is partly supported by Jiangsu Province Natural Science Foundation (Young Talent Program No. BK20130573), "333" project of Jiangsu Province (BRA2015284) and National Basic Research 973 Program under Grants 2014CB921101, 2013CB932900, 2013CB632101, 2010CB934402 and NSFC under Nos. 11274155 and 61204050. Scientific and Technological Support Programme in Jiangsu province under No. BE2014147-2, Jiangsu Shuang chuang Personal/Team's Program and the Fundamental Research Funds for the Central Universities.

Appendix A. Supplementary material

Supplementary data associated with this article can be found in the online version at http://dx.doi.org/10.1016/j.nanoen.2015.10.031.

References

[1] M. Armand, J.-M. Tarascon, Nature 451 (2008) 652-657.
[2] D. Larcher, J. Tarascon, Nat. Chem. (2014).
[3] M.N. Obrovac, L. Christensen, Electrochem. Solid.ST. 7 (2004) A93.
[4] K. Kravchyk, L. Protesescu, M.I. Bodnarchuk, F. Krumeich, M. Yarema, M. Walter, C. Guntlin, M.V. Kovalenko, J. Am. Chem. Soc. 135 (2013) 4199-4202.
[5] N. Liu, H. Wu, M.T. McDowell, Y. Yao, C. Wang, Y. Cui, Nano Lett. 12 (2012) 3315-3321.
[6] X.W. Zhang, S.B. Lin, T. Lin, P. Zhang, J. Xu, L. Xu, K.J. Cheng, Phys. Chem. Chem. Phys. 17 (2015) 11974-11980.

[7] A. Nie, L.-Y. Gan, Y. Cheng, H. Asayesh-Ardakani, Q. Li, C. Dong, R. Tao, F. Mashayek, H.-T. Wang, U. Schwingenschlögl, ACS Nano 7 (2013) 6203–6211.
[8] E. Mullane, T. Kennedy, H. Geaney, C. Dickinson, K.M. Ryan, Chem. Mater. 25 (2013) 1816–1822.
[9] C.K. Chan, H. Peng, G. Liu, K. McIlwrath, X.F. Zhang, R. A. Huggins, Y. Cui, Nat. Nanotechnol. 3 (2008) 31–35.
[10] J.Y. Huang, L. Zhong, C.M. Wang, J.P. Sullivan, W. Xu, L. Q. Zhang, S.X. Mao, N.S. Hudak, X.H. Liu, A. Subramanian, H. Fan, L. Qi, A. Kushima, J. Li, Science 330 (2010) 1515–1520.
[11] J. Wang, N. Du, H. Zhang, J. Yu, D. Yang, J. Phys. Chem. C 115 (2011) 11302–11305.
[12] T. Song, J. Xia, J.H. Lee, D.H. Lee, M.S. Kwon, J.M. Choi, J. Wu, S.K. Doo, H. Chang, W.I. Park, D.S. Zang, H. Kim, Y. Huang, K.C. Hwang, J.A. Rogers, U. Paik, Nano Lett. 10 (2010) 1710–1716.
[13] J. Deng, C. Yan, L. Yang, S. Baunack, S. Oswald, H. Wendrock, Y. Mei, O.G. Schmidt, ACS Nano 7 (2013) 6948–6954.
[14] C. Wang, G. Du, K. Ståhl, H. Huang, Y. Zhong, J.Z. Jiang, J. Phys. Chem. C 116 (2012) 4000–4011.
[15] M.T. McDowell, S.W. Lee, W.D. Nix, Y. Cui, Adv. Mater. 25 (2013) 4966–4985.
[16] A.L. Mohana Reddy, S.R. Gowda, M.M. Shaijumon, P.M. Ajayan, Adv. Mater. 24 (2012) 5045–5064.
[17] A. Magasinski, P. Dixon, B. Hertzberg, A. Kvit, J. Ayala, G. Yushin, Nat. Mater. 9 (2010) 353–358.
[18] B. Liu, X. Wang, H. Chen, Z. Wang, D. Chen, Y.B. Cheng, C. Zhou, G. Shen, Sci. Rep. 3 (2013) 1622.
[19] L.-F. Cui, R. Ruffo, C.K. Chan, H. Peng, Y. Cui, Nano Lett. 9 (2008) 491–495.
[20] L.-F. Cui, Y. Yang, C.-M. Hsu, Y. Cui, Nano Lett. 9 (2009) 3370–3374.
[21] D.-W. Kim, I.-S. Hwang, S.J. Kwon, H.-Y. Kang, K.-S. Park, Y.-J. Choi, K.-J. Choi, J.-G. Park, Nano Lett. 7 (2007) 3041–3045.
[22] P. Meduri, C. Pendyala, V. Kumar, G.U. Sumanasekera, M. K. Sunkara, Nano Lett. 9 (2009) 612–616.
[23] J. Yan, A. Sumboja, E. Khoo, P.S. Lee, Adv. Mater. 23 (2011) 746–750.
[24] W. Zhou, C. Cheng, J. Liu, Y.Y. Tay, J. Jiang, X. Jia, J. Zhang, H. Gong, H.H. Hng, T. Yu, H.J. Fan, Adv. Funct. Mater. 21 (2011) 2439–2445.
[25] Y. Cui, L.J. Lauhon, M.S. Gudiksen, J. Wang, C.M. Lieber, Appl. Phys. Lett. 78 (2001) 2214.
[26] L. Yu, P.J. Alet, G. Picardi, I. Maurin, P.R. Cabarrocas, Nanotechnology 19 (2008) 485605.
[27] W. Ren, C. Wang, L. Lu, D. Li, C. Cheng, J. Liu, J. Mater. Chem. A 1 (2013) 13433–13438.
[28] C. Guan, X. Wang, Q. Zhang, Z. Fan, H. Zhang, H.J. Fan, Nano Lett. 14 (2014) 4852–4858.
[29] J.-H. Jeun, K.-Y. Park, D.-H. Kim, W.-S. Kim, H.-C. Kim, B.-S. Lee, H. Kim, W.-R. Yu, K. Kang, S.-H. Hong, Nanoscale 5 (2013) 8480–8483.
[30] J.W. Choi, J. McDonough, S. Jeong, J.S. Yoo, C.K. Chan, Y. Cui, Nano Lett. 10 (2010) 1409–1413.
[31] T. Kennedy, E. Mullane, H. Geaney, M. Osiak, C. Dwyer, K. M. Ryan, Nano Lett. 14 (2014) 716–723.
[32] W. Zeng, F. Zheng, R. Li, Y. Zhan, Y. Li, J. Liu, Nanoscale 4 (2012) 2760–2765.
[33] J. Liu, Y. Li, X. Huang, R. Ding, Y. Hu, J. Jiang, L. Liao, J. Mater. Chem. 19 (2009)1859 19 (2009).
[34] Y.D. Ko, J.G. Kang, J.G. Park, S. Lee, D.W. Kim, Nanotechnology 20 (2009) 455701.
[35] J.M. Haag, G. Pattanaik, M.F. Durstock, Adv. Mater. 25 (2013) 3238–3243.
[36] W. Ren, C. Wang, L. Lu, D. Li, C. Cheng, J. Liu, J. Mater. Chem. A 1 (2013) 13433.
[37] S. Jing, H. Jiang, Y. Hu, C. Li, J. Mater. Chem. A 2 (2014) 16360–16364.
[38] Q. Xiao, Y. Fan, X. Wang, R.A. Susantyoko, Q. Zhang, Energy Environ. Sci. 7 (2014) 655–661.
[39] W. Wang, M. Tian, Y. Wei, S.-H. Lee, Y.-C. Lee, R. Yang, Nano Energy. 2 (2013) 943–950.
[40] N. Liu, Z.D. Lu, J. Zhao, M.T. McDowell, H.-W. Lee, W.T. Zhao, Y. Cui, Nat. Nanotechnol. 9 (2014) 187–192.
[41] J.X. Song, M.J. Zhou, R. Yi, T. Xu, M.L. Gordin, D.H. Tang, Z. X. Yu, M. Regula, D.H. Wang, Adv. Funct. Mater. 24 (2014) 5904–5910.
[42] H. Zhao, N. Yuca, Z.Y. Zheng, Y.B. Fu, V.S. Battaglia, G. Abdelbast, K. Zaghib, G. Liu, ACS Appl. Mater. Interfaces 7 (2015) 862–866.

Hucheng Song received his M.S. degrees in key laboratory for special functional materials from Henan University in 2013. He is currently a Ph.D. candidate of the School of Electronic Engineering, Nanjing University, China. His research interests mainly focus on design and fabrication of lithium ion battery anode material with high capacity including silicon (Si), Germanium (Ge) and Metallic oxide.

Hongxiang Wang is a master student at National Laboratory of Solid State Microstructures and School of Electronics Science and Engineering/Collaborative Innovation Center of Advanced Microstructures, Nanjing University of China. His research focuses on nano-composite silicon-based anode materials for lithium ion batteries

Xiaofan Jiang received the B.S. and M.S. degrees in school of physics from Nanjing University, Nanjing, China, in 2009 and 2012, respectively, where he is currently pursuing the Ph.D. degree in electronic science and technology. His current research interests include the Si-based resistive switching memory and quantum dot floating-gate memory devices.

Linwei Yu received the B.S. degree in semiconductor physics in 2001 and the Ph. D. degree in microelectronics from Nanjing University, Nanjing, China, in 2007. From 2007 to 2009, he was a Postdoctoral Researcher with LPICM, Ecole Polytechnique, France, and joined CNRS as a Permanent Researcher (CR2) in 2009. Since 2013, he has been a Professor with the School of Electronics Science and Engineering, Nanjing University. His research interests include the growth mechanism and application of semiconductor nanostructures for large-scale thin film electronics, battery and advanced photovoltaic technologies.

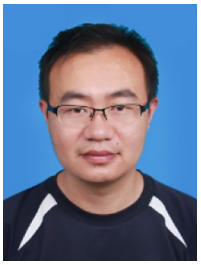

Zhongwei Yu received his B.S. degree in Nanjing Normal University in 2002 and M.S. degree in the School of physics from Suzhou University in 2007. He is currently a Ph.D. candidate of the School of Electronic Engineering, Nanjing University, China. His research interests mainly focus on the growth mechanism and application of advanced silicon nanostructures.

Jun Xu received the B.S. degree in physics and the Ph.D. degree in microelectronics both from Nanjing University, Nanjing, China, in 1989 and 1995, respectively. In 1996, he was a member of the National Laboratory of Solid State Microstructures, Nanjing University. Since 2004, he has been a Professor in the Department of Phyics and School of Electronic Science and Engineering. He worked as a Visiting Researcher in the Department of Electronic Engineering, Hongkong Chinese University, in 2000 and the Graduate School of Advanced Science of Matter, Hiroshima University, Japan, in 2005. His research interests include silicon-based amorphous materials, semiconductor nanostructures, and optoelectronic devices.

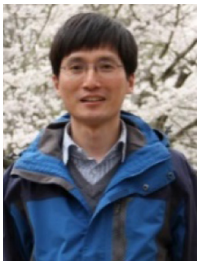

Mingbo Zheng received his Ph.D. in material processing engineering from Nanjing University of Aeronautics and Astronautics in 2009. He was a postdoctoral researcher at Nanjing University from 2009 to 2012. He was an associate researcher at Nanjing University from 2012 to 2015. He is currently an associate professor at Yanzhou University. His research interests are in the field of materials for energy storage, including lithium-ion battery, lithium-sulfur battery, lithium-air battery, and supercapacitor.

Lijia Pan is a full Professor of the School of Electronic Engineering, Nanjing University, China. He received his B.S. degree in department of polymer science and engineering from South China University of Technology, and obtained Ph.D. of polymer physics from University of Science and Technology of China in 2003. He did three years postdoctoral research in the Physics Department of Nanjing University, and then worked as an associate professor in the Physics Department of Nanjing University in 2007. He visited Prof. Zhenan Bao's group at Stanford University as a visiting scholar in 2011-2012. His research interests include: 1) Intelligent materials and devices; 2) Bionic electronics; 3) Advanced energy storage and conversion materials.

Kunji Chen received the Graduate degree from Nanjing University, Nanjing, China, in 1963.From 1981–1983, he was a Visiting Scholar studying at the University of Chicago, Chicago, IL, USA. Since then he had eight times to go to the Universities and Institutes of United State and Japan for cooperation research work. He is currently a Professor at Nanjing University. His research interests include nanosemiconductor materials, quantum nanoelectronics, and nanooptoelectronics. Prof. Chen has received many awards including the National Nature Science Award in 2003 and the Advanced Achievements Award in Science and Technology of Jiangsu Province (1988, 1995, and 2002). In 1996, he was elected as a member of the International Advisory Committee of International Conference on Amorphous and Nanocrystalline Semiconductors (ICANS).

Yi SHI received the Ph.D. in Physics from Nanjing University, China, in 1989. He joined Nanjing University as an Assistant Professor in 1989, became an Associate Professor in 1993, and a Professor in 1996. He is a recipient of the 2002 outstanding young Chinese scientist award from the National Science Foundation of China. Since 2006, he is a Changjiang professor at Nanjing University. Dr. SHI has published on advanced electronic and optoelectronic materials and devices as well as on nanotechnology in professional journals (>300) and conferences (>30). Currently, his research interests are focused on nanostructured materials and the applications in optoelectronics and energy.

Zixia Lin is an post doctor in School of Electronic Science and Engineering at Nanjing University.
He received his B.Sc. (2006) and Ph.D. (2013) in Microelectronics and Solid-state Electronics(2006), from Nanjing University (Nanjing, China). His current research interests are rechargeable lithium-ion battery, Li-Air battery, mesoporous nano materials.